Knotted Defects in Nematic Liquid Crystals

Thomas Machon and Gareth P. Alexander
Department of Physics and Centre for Complexity Science, University of Warwick, Coventry CV4 7AL, United Kingdom
(Received 27 February 2014; published 9 July 2014)

We show that the number of distinct topological states associated with a given knotted defect, L, in a nematic liquid crystal is equal to the determinant of the link L. We give an interpretation of these states, demonstrate how they may be identified in experiments, and describe the consequences for material behavior and interactions between multiple knots. We show that stable knots can be created in a bulk cholesteric and illustrate the topology by classifying a simulated Hopf link. In addition, we give a topological heuristic for the resolution of strand crossings in defect coarsening processes which allows us to distinguish topological classes of a given link and to make predictions about defect crossings in nematic liquid crystals.

DOI: 10.1103/PhysRevLett.113.027801 PACS numbers: 61.30.Jf, 02.10.Kn, 02.40.Re

Topological concepts have come to play an increasingly significant role in characterizing and controlling material behavior across all areas of condensed matter, encompassing vortices in fluids [1,2], defects in ordered media [3–5], the quantum Hall effect [6,7], colloids in liquid crystals [8–11], topological insulators [12,13], and boundary modes in isostatic lattices [14,15]. A recent development has been the experimental creation of knotted field configurations in laser light [16], liquid crystals [11,17–20], and fluid flows [21], leading to a resurgence of theoretical interest in electromagnetism [22–25], superfluids [26], liquid crystals [27], and particle physics [28]. In liquid crystals, knotted fields are often produced, or controlled, by colloidal particles and their associated topological defects [11,17,27]. By suitable manipulation with laser tweezers, the defect lines can be tied into arbitrary knots and links [17,29]. Furthermore, modern fabrication techniques allow the colloids themselves to be made in the shape of a knot [20], including with hybrid surface anchoring conditions [19], so that the colloid faithfully mimics a defect line. Thus, more or less arbitrary knotted textures can be made and manipulated, and it is important to understand and characterize their properties.

Knots are intricate entities that display enormous diversity. Different knots, and links, distinguish themselves through a large number of topological invariants, including various polynomials, homology groups, and homotopy groups [30,31]. These must be encoded in any knotted field, although, at present, it is almost completely unknown which invariants manifest themselves in distinct material properties or behavior. A most basic question is how to determine how many topologically distinct knotted configurations are compatible with a given link, L, and characterize them. For instance, there are an infinite number of distinct point vortices in the XY model labelled by an integer winding number, and the distinct types of topological insulators and superconductors can be classified by a periodic table using Bott periodicity [32]. Here, we show that the number of distinct knotted fields in a nematic liquid crystal (up to homotopy) is given by the determinant of the link, a well-known and readily computable knot invariant. Thus, the number of Hopf link textures is two, the number of trefoil knots is three, and the number of Borromean rings is sixteen. All of these links have been created experimentally [17]; our result begs the question of which ones? We characterize experimental signatures of all of these textures, accessible using three-photon excitation fluorescence polarizing microscopy [18] or direct observations of strand crossing [33,34]. Finally, we demonstrate, numerically, that many different links can appear as free-standing metastable textures in bulk cholesterics.

Defect lines in nematics, whether genuine or imitated by colloids [19], are regions where the material order is undefined and are characterized by the property that the molecular alignment reverses orientation upon going around the line once [35]. This gives a vivid visual demonstration that the order in nematics corresponds to a unit line field, called the director, rather than a vector. Nonetheless, it is a widely adopted convention to treat the director as a vector field and impose the equivalence $n \sim -n$ "by hand." A formal treatment of this process provides a natural framework for characterizing knotted nematics. Since the alignment returns to the same orientation upon going around the disclination twice, any knotted director field, n, can be lifted to a vector field, $\hat{n}$, on the cyclic double cover $\hat{\Sigma}(L)$ of the link complement, a process analogous with the familiar branch cuts of complex analysis. It is the topology of this space that is explored by the nematic, which provides a physical realization of the double branched cover of S^3 over the link. This perspective allows the director to be properly treated as a global vector field, the topology of which is classified by standard tools in homology theory [36].

To outline, briefly, how our classification result follows: after passing to the vector field $\hat{n}$, the equivalence relation $n \sim -n$ is restated as a compatibility condition with respect to the deck transformation, t, of the covering space (that moves us from a point x on one sheet of the cover to the equivalent point of the other)

$$\hat{n}(tx) = -\hat{n}(x). \tag{1}$$

Such vector fields are said to be equivariant. Before imposing equivariance, unit vector fields on the cyclic double cover are classified by the induced map on second cohomology and, hence, by the group $H^2(\hat{\Sigma}(L)) \cong H_1(\hat{\Sigma}(L), \partial\hat{\Sigma}(L))$ [37]. The elements of this group are cycles that entangle the knot and tethers that connect various link components, illustrated in Fig. 2. Restricting to equivariant maps only allows cycles of the form $(e - te)$. Equivalence between a pair of cycles $(e - te)$ and $(e' - te')$ is established by considering equivariant homotopies that exchange cycles across any branching surface between the two sheets of $\hat{\Sigma}(L)$. These conditions reduce the group $H_1(\hat{\Sigma}(L), \partial\hat{\Sigma}(L))$ to $H_1(\Sigma(L))$, the first homology group of the double branched cover of S^3 over L. The order of this group (if finite) is known as the knot determinant and counts the number of topologically distinct nematic textures associated to a given link, L [38]. In addition to a finite number of states for knots (see Fig. 1), some links support an infinite number of states, the (4,4) torus link [see Fig. 1(c)], for example, has $H_1(\Sigma(L)) = \mathbb{Z}_2 \oplus \mathbb{Z}^2$, meaning that the state is described by three integers, one of which is defined mod 2.

We can use this result to understand the topology of multiple knotted and linked defects in a nematic. If a given link L is split (meaning that it has multiple components that can each be surrounded by a measuring sphere in the space) into say $L_1, \ldots, L_n$, shown in Fig. 1(a), then $H_1(\Sigma(L))$ splits as a direct sum [30]

$$H_1(\Sigma(L)) = \mathbb{Z}^{n-1} \oplus \left(\bigoplus_{i=1}^{n} H_1(\Sigma(L_i)) \right). \tag{2}$$

This equation encodes the topological interaction between a collection of knots and links. Indeed, one can think of each split component as a knotted "particle," the internal states of which are given by $H_1(\Sigma(L_i))$, i.e., the determinant of the component on its own. This interpretation, reminiscent of Kelvin's "vortex atoms" [40], is supplemented by a topological interaction between the components. This is specified by an integer associated to each component, interpreted as the usual "hedgehog charge" that identifies point defects. This gives the factor of $\mathbb{Z}^{n-1}$ in (2), there being only $n-1$ degrees of freedom due to the conserved total charge imposed by the uniform far-field boundary conditions. Each factor of $\mathbb{Z}$ can be calculated in the usual way by considering the director field on a measuring sphere and computing the degree of the map [35,39].

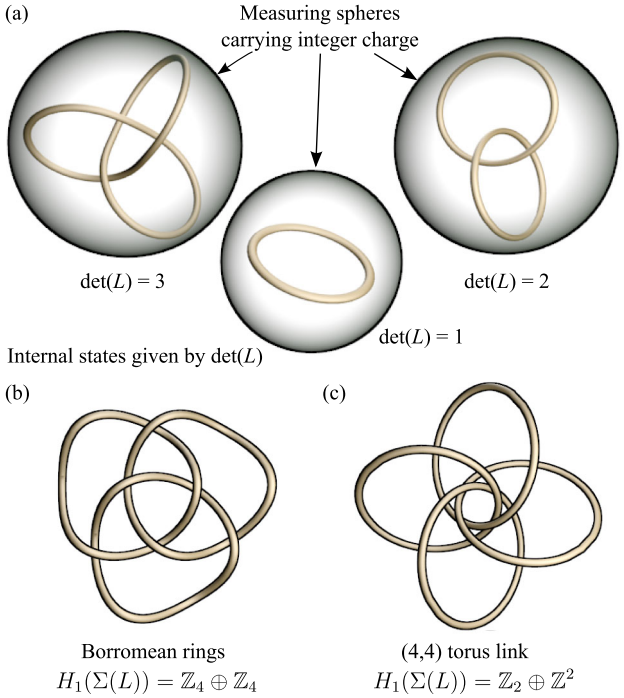

FIG. 1 (color online). (a) "Particle" based picture of knotted defects in liquid crystals. Each link ($L - R$: trefoil knot, unknot, and Hopf link) has an internal degree of freedom given by an element of $H_1(\Sigma(L))$, the size of which is $\det(L)$. Each split component then carries a hedgehog charge, calculated using the degree of the texture on the measuring spheres [35,39], which is constrained by charge conservation. (b) Borromean rings; for this link $H_1(\Sigma(L)) = \mathbb{Z}_4 \oplus \mathbb{Z}_4$ giving a total of 16 distinct states. (c) (4,4) torus link; this link has $H_1(\Sigma(L)) = \mathbb{Z}_2 \oplus \mathbb{Z}^2$, and, thus, supports an infinite number of states.

To complement this topological classification, we give a physical interpretation of these states and describe methods to identify knots produced experimentally or in simulation. This is provided by the Pontryagin-Thom (PT) construction, illustrated in Fig. 2, which allows the different states to be distinguished by a combination of "Skyrmion tubes" and relative disclination orientation. This construction has been implemented experimentally [18], and its employment should enable the identification of knotted defects in the laboratory. The PT construction gives a rigorous and succinct way of viewing the global topological data encoded in a director field [41,42]. One draws the surface consisting of all points where the director is perpendicular to a chosen orientation $\mathbf{d}$. For a given $\mathbf{d}$, any π rotation of the director will be perpendicular to $\mathbf{d}$ at least once and so, for line defects, this construction produces a surface whose boundaries are disclination lines, shown in Fig. 2(d). An additional degree of freedom, corresponding to the director orientation in the plane perpendicular to $\mathbf{d}$, is used to color the surface, as in Fig. 2(b). While the PT surface need not

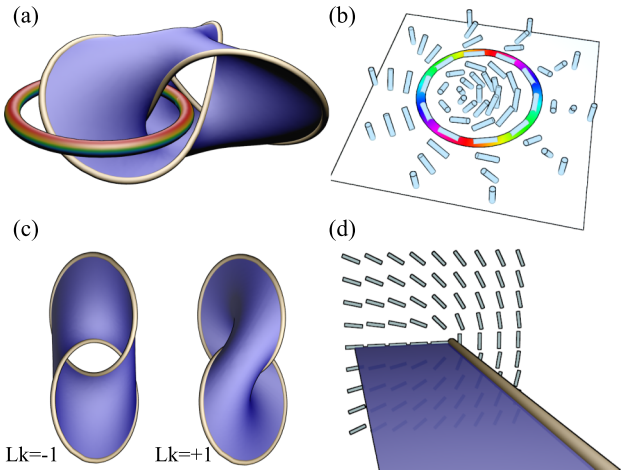

FIG. 2 (color online). Using the Pontryagin-Thom construction to understand knotted textures. (a) Cartoon PT surface (blue) for a trefoil knot, entangled with a Skyrmion tube. The tube cannot be removed without altering the topology of the defect line; the number of these tubes distinguishes the different topological classes. The shading (coloring) of the Skyrmion tube corresponds to the shading (coloring) of the strip in (b). (b) Cartoon showing the relation between a Skyrmion (tube) and the PT surface. The surface is drawn where the director is horizontal, and shaded (colored) by orientation as shown. (c) The two distinct Hopf link textures can be distinguished by the structure of their potential PT surfaces. Using the right-hand rule, one can define an orientation for each link and compute linking numbers. The $\mathrm{Lk} = +1$ texture is also equivalent to the $\mathrm{Lk} = -1$ texture with an additional tether connecting the two components. (d) The Pontryagin-Thom surface. The surface is constructed as the set of all points where the molecular orientation is perpendicular to a chosen direction **d**; disclinations become boundaries of this surface.

be orientable, the direction in which the director rotates as one lifts off the surface defines a local orientation on the PT surface, which can be reversed through a π rotation of the director in the surface itself [43].

In terms of this construction, the difference between states is captured by differences in the topology and coloring of this surface. For a knot or link, the PT construction produces a surface, F, whose boundary is L, demonstrated in Figs. 2(a) and 2(c). This F corresponds to a "branch cut" between the two sheets that was performed during the transition to $\hat{\Sigma}(L)$. In Fig. 2, this surface is shown in blue, the constant color indicating that the orientation of the director on the surface is uniform. Textures also exist where the surface F does not have a constant color. In these cases, one can perform a deformation of the texture, corresponding to a cobordism of the surface, contracting the region of color winding and pulling the colored part of the surface away from F, until it takes the form of separate pieces of surface that are either tubes entangled with the surface as shown in Fig. 2(a), or tethers joining separate link components. These tubes or tethers have a 2π winding of the director around their meridian and can be thought of as Skyrmion tubes, a baby Skyrmion, with a profile as in Fig. 2(b), extruded along a cycle. The cycle along which this tether or tube runs is precisely a cycle in $H_1(\hat{\Sigma}(L), \partial\hat{\Sigma}(L))$, giving a vivid visual correspondence between the classification and physical realization of these textures.

An additional subtlety arises for links, which may support multiple topologically distinct planar textures, i.e., the director lies everywhere in a single plane (the $(x\text{-}z)$ plane, say). Such textures do not possess any Skyrmion tubes. Figure 2(c) furnishes an example of this, demonstrating representatives of the two distinct textures that may be associated to the Hopf link. These examples have interpretations as disclinations with linking number $\mathrm{Lk} = \pm 1$.

This topological distinction manifests itself in the physical behavior of defect lines. A free-standing defect in a nematic will coarsen over time, undergoing strand crossings in order to reduce its free energy [33,34]. Such strand crossings have long been expected to have a distinctive topological character in systems with a non-Abelian fundamental group [44] but have never been observed. In the light of our topological classification, we find that the behavior and relaxation of unstable defects has a similarly distinctive dependence on the topological class of the knot or link. We demonstrate this using the Hopf link, though the phenomenon is general in nature, with relevance to all defect crossing processes. Figure 3 shows simulated relaxation dynamics of two Hopf link defects, with linking numbers ± 1. The resolution of strand crossings in such relaxation processes is observed to always preserve the

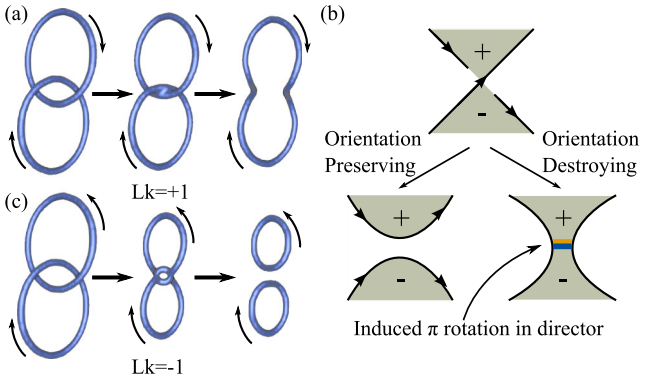

FIG. 3 (color online). The topology of defect crossing processes. (a) and (c) Simulation results showing example relaxations of $\mathrm{Lk} = +1$ and $\mathrm{Lk} = -1$ Hopf link textures. The orientation induced by the PT surface, shown by black arrows, is preserved by the strand crossings. (b) Schematic of a possible defect strand cobordism. The Pontryagin-Thom surface is shown shaded. The orientation destroying resolution necessarily induces a π rotation of the director in the surface, indicated by the colored bar; this distortion is energetically unfavored in a nematic, and so, in such systems, the resolution will preserve the orientation induced by the PT surface.

effective orientation imparted to the defects by the Pontryagin-Thom surface [shown in Fig. 2(c)]. This effect can be understood as a combination of energetics and topology. The simplification of defect lines can be pictured in terms of elementary cobordism moves, an example of which is shown in Fig. 3(b). These cobordism moves act not just on the defects themselves but on the defects and the PT surface simultaneously, a reflection of the fact that the entire nematic texture is knotted, not just the disclinations. Locally the sides of the PT surface are distinguished, and for a cobordism to connect the two opposite sides (and facilitate a strand crossing) requires a local π rotation in the director on the surface itself. This π rotation is topologically required only if the cobordism does not preserve orientation. Since the energy in a nematic is a simple quadratic elasticity, such distortions as produced by the orientation destroying cobordism are suppressed.

This behavior provides a means to distinguish the topological types of links and knots purely by observation. For example, the two distinct Hopf links may be distinguished by the manner in which they annihilate, as in Fig. 3. More generally, this gives an initial characterization of the topological dynamics of defects in nematic systems. Indeed, the outcome of generic defect processes, easily observed experimentally, can be predicted by this rule.

What of the influence of topology on stable knotted configurations? The natural setting for stable knots is either in colloidal systems [17,19,20,27] or in cholesterics, where one can exploit the length scale set by the cholesteric pitch. This has been demonstrated in simulations of cholesteric droplets [45] and unknotted configurations in strong confinement [46], but never knots in bulk materials without the presence of colloidal particles. Here, we show numerically the existence of a stable Hopf link in a bulk cholesteric, shown in Fig. 4. Using the PT construction, we are able to extract the topological class of the configuration, demonstrating a possible experimental method of identification. Figures 4(a) and 4(c) show a stable $\mathrm{Lk} = +1$ Hopf link, while Fig. 4(b) shows the PT surface computed from the simulation results. The defect lines are of order one pitch length in size, and display a local twist profile in the director. The PT surface is orientable, and carries no color winding, Skyrmion tethers, or tubes. We may, therefore, use the induced orientation on the boundary components to compute the linking number of the defect lines and identify the state. While Fig. 4 shows only a Hopf link, we have also been able to stabilize a large variety of knots and links—such as the trefoil, figure eight, and Solomon's knot—limited only by our persistence. The simulation shown has $q_0 < 0$ and it is interesting to note that the $\mathrm{Lk} = -1$ Hopf link was only found to be stable with $q_0 > 0$, with a similar phenomenon shown for the left- and right-handed trefoil knots, suggesting a link between the chirality of the system and of the knot.

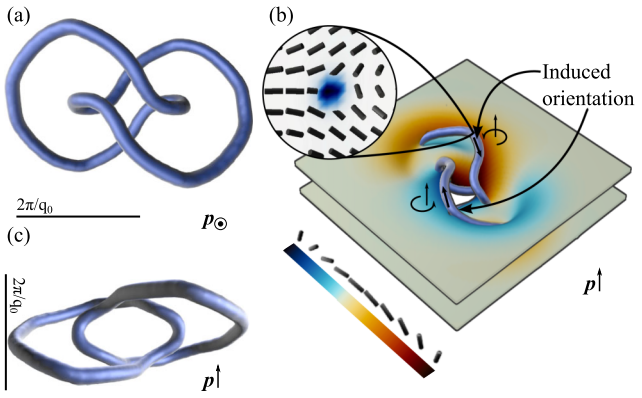

FIG. 4 (color online). Simulation results showing metastable $\mathrm{Lk} = +1$ Hopf link in a cholesteric, found by numerical relaxation of the Landau–de Gennes free energy. (a) and (c) Vertical and horizontal views of the knotted configuration; the pitch direction is denoted by **p**. Note that the size of the defects is comparable to $2\pi/q_0$. (b) PT surface plotted from simulation results. The two sheets correspond to a bulk cholesteric in which the link is embedded. The topological class of the link can be found by looking at the induced orientation on the link components by the PT surface and then computing the linking number. The legend at the bottom shows the relationship between surface coloring and director orientation. The inset shows the twist profile of the disclinations.

To make controlled simulations of these states, in both the nematic and cholesteric cases, we use Milnor fibrations [47] to construct an ansatz containing a knotted director field. These have also been used in optics [16] and electromagnetism [25], so we merely summarize the features relevant to the present construction. We take the complex polynomial $f(z_1, z_2) = z_1^p + (-iz_2)^q$ restricted to $S^3 \subset \mathbb{C}^2$, i.e., $|z_1|^2 + |z_2|^2 = 1$. Constructing the director ansatz

$$n = (\cos(q_0 z + \phi/2), \sin(q_0 z + \phi/2), 0), \qquad (3)$$

where $\phi(\vec{x})$ is the argument of the stereographic projection of f into $\mathbb{R}^3$, gives a director field containing a defect in the form of a (p, q) torus knot embedded into a standard cholesteric texture (or nematic for $q_0 = 0$). While the polynomial given only generates torus knots, an extension to other polynomials [16,48] may be used to generate an entire zoo of knots and links. Furthermore, the texture of (3) is planar, and cannot correspond to a topological class containing Skyrmion tubes; these additional topological classes may be produced by a generalization involving appropriate meromorphic functions [49]. The topologically distinct planar textures for links may be constructed using conjugated polynomials [49,50]. For example, the choices $(z_1 + z_2)(z_1 - z_2)$ and $(z_1 + z_2)\overline{(z_2 - z_1)}$ give planar representatives of the $\mathrm{Lk} = +1$ and $\mathrm{Lk} = -1$ textures for the Hopf link, respectively [51]. To simulate the system, we use

the standard Landau-de Gennes theory. We embed the director into a Q tensor as $Q = s(n \otimes n - \frac{1}{3}\mathbb{I})$ and take the relaxation dynamics $\partial_t Q = -\Gamma(\delta F/\delta Q)$, where F is the standard Landau–de Gennes free energy [52]. The simulations were run on a 192^3 grid with typical parameter values.

This work was partially supported by the EPSRC. T. M. was also partially supported by a University of Warwick Chancellor's Scholarship.

[1] L. Woltjer, Proc. Natl. Acad. Sci. U.S.A., **44**, 489 (1958).
[2] H. K. Moffatt, J. Fluid Mech. **35**, 117 (1969).
[3] G. Toulouse and M. Kléman, J. Phys. Lett. **37**, 149 (1976).
[4] G. E. Volovik and V. P. Mineev, Pis'ma Zh. Exp. Teor. Fiz **24**, 605 (1976) [JETP Lett. **24**, 561 (1976)].
[5] M. Kléman, L. Michel, and G. Toulouse, J. Phys. Lett. **38**, 195 (1977).
[6] K. von Klitzing, G. Dorda, and M. Pepper, Phys. Rev. Lett. **45**, 494 (1980).
[7] D. J. Thouless, M. Kohmoto, M. P. Nightingale, and M. den Nijs, Phys. Rev. Lett. **49**, 405 (1982).
[8] E. M. Terentjev, Phys. Rev. E **51**, 1330 (1995).
[9] P. Poulin, H. Stark, T. C. Lubensky, and D. A. Weitz, Science **275**, 1770 (1997).
[10] I. Muševič, M. Škarabot, U. Tkalec, M. Ravnik, and S. Žumer, Science **313**, 954 (2006).
[11] B. Senyuk, Q. Liu, S. He, R. D. Kamien, R. B. Kusner, T. C. Lubensky, and I. I. Smalyukh, Nature (London) **493**, 200 (2013).
[12] C. L. Kane and E. J. Mele, Phys. Rev. Lett. **95**, 146802 (2005).
[13] M. Z. Hasan and C. L. Kane, Rev. Mod. Phys. **82**, 3045 (2010).
[14] K. Sun, A. Souslov, X. Mao, and T. C. Lubensky, Proc. Natl. Acad. Sci. U.S.A. **109**, 12369 (2012).
[15] C. L. Kane and T. C. Lubensky, Nat. Phys. **10**, 39 (2013).
[16] M. R. Dennis, R. P. King, B. Jack, K. O'Holleran, and M. J. Padgett, Nat. Phys. **6**, 118 (2010).
[17] U. Tkalec, M. Ravnik, S. Čopar, S. Žumer, and I. Muševič, Science **333**, 62 (2011).
[18] B. G. Chen, P. J. Ackerman, G. P. Alexander, R. D. Kamien, and I. I. Smaluykh, Phys. Rev. Lett. **110**, 237801 (2013).
[19] M. Cavallaro, Jr., M. A. Gharbi, D. A. Beller, S. Čopar, Z. Shi, R. D. Kamien, S. Yang, T. Baumgart, and K. J. Stebe, Soft Matter **9**, 9099 (2013).
[20] A. Martinez, M. Ravnik, B. Lucero, R. Visvanathan, S. Žumer, and I. I. Smalyukh, Nat. Mater. **13**, 258 (2014).
[21] D. Kleckner and W. T. M. Irvine, Nat. Phys. **9**, 253 (2013).
[22] A. F. Rañada, J. Phys. A **25**, 1621 (1992).
[23] W. T. M. Irvine and D. Bouwmeester, Nat. Phys. **4**, 716 (2008).
[24] W. T. M. Irvine, J. Phys. A **43**, 385203 (2010).
[25] H. Kedia, I. Bialynicki-Birula, D. Peralta-Salas, and W. T. M. Irvine, Phys. Rev. Lett. **111**, 150404 (2013).
[26] D. Proment, M. Onorato, and C. F. Barenghi, Phys. Rev. E **85**, 036306 (2012).
[27] T. Machon and G. P. Alexander, Proc. Natl. Acad. Sci. U.S.A. **110**, 14174 (2013).
[28] P. M. Sutcliffe, Proc. R. Soc. A **463**, 3001 (2007).
[29] R. D. Kamien, Science **333**, 46 (2011).
[30] D. Rolfsen, *Knots and Links* (AMS Chelsea Publishing, Providence, 2003).
[31] W. B. R. Lickorish, *An Introduction to Knot Theory* (Springer, New York, 1997).
[32] A. Kitaev, arXiv:0901.2686v2.
[33] I. Chuang, R. Durrer, N. Turok, and B. Yurke, Science **251**, 1336 (1991).
[34] T. Ishikawa and O. D. Lavrentovich, Europhys. Lett. **41**, 171 (1998).
[35] G. P. Alexander, B. G. Chen, E. A. Matsumoto, and R. D. Kamien, Rev. Mod. Phys. **84**, 497 (2012).
[36] A. Hatcher, *Algebraic Topology* (Cambridge University Press, Cambridge, England, 2001).
[37] H. Whitney, Duke Math. J. **3**, 51 (1937).
[38] Allowing the action of $\pi_1(\mathbb{RP}^2)$ on $\pi_2(\mathbb{RP}^2)$ reduces the number of distinct textures to $H_1(\Sigma(L))/(x \sim -x)$.
[39] N. D. Mermin, Rev. Mod. Phys. **51**, 591 (1979).
[40] W. Thomson, Proc. R. Soc. Edinburgh, Sect. A **6**, 94 (1867).
[41] T. tom Dieck, *Algebraic Topology* (European Mathematical Society, Zürich, 2008).
[42] B. G. Chen, Ph.D. thesis, University of Pennsylvania, 2012.
[43] Technically, the requirement is for a consistent map from the normal bundle of the PT surface into the normal bundle of the circle in $\mathbb{RP}^2$ defined by $\mathbf{d}$.
[44] V. Poénaru and G. Toulouse, J. Phys. (Paris) **38**, 887 (1977).
[45] D. Seč, S. Čopar, and S. Žumer, Nat. Commun. **5**, 3057 (2014).
[46] J. I. Fukuda and S. Žumer, Phys. Rev. Lett. **106**, 097801 (2011).
[47] J. Milnor, *Singular Points of Complex Hypersurfaces* (Princeton University Press, Princeton, 1968).
[48] A. Rémond-Tiedrez, T. Wan, T. Machon, and G. P. Alexander (to be published).
[49] T. Machon and G. P. Alexander, arXiv:1307.6819v3.
[50] J. Seade, *On the Topology of Isolated Singularities in Analytic Spaces* (Birkhäuser Verlag, Basel, 2006).
[51] Note that, as polynomials, they have the same zero set and, thus, disclinations with identical geometry.
[52] M. Ravnik and S. Žumer, Liq. Cryst. **36**, 1201 (2009).